remote sensing

MDPI

Article

Joint Prediction of Sea Clutter Amplitude Distribution Based on a One-Dimensional Convolutional Neural Network with Multi-Task Learning

Longshuai Wang [1], Liwen Ma [1,*], Tao Wu [2], Jiaji Wu [3] and Xiang Luo [4]

[1] College of Computer Science & Technology, Qingdao University, Qingdao 266071, China; wanglongshuai@qdu.edu.cn
[2] Xi'an Institute of Space Radio Technology, Xi'an 710100, China; wut1@cast504.com
[3] School of Electronic Engineering, Xidian University, Xi'an 710071, China; wujj@mail.xidian.edu.cn
[4] Wuhan Wisdom Bio-Technology Co., Ltd., Wuhan 430000, China; luoxiang@smart-view.com.cn
* Correspondence: malw@qdu.edu.cn

Abstract: Accurate modeling of sea clutter amplitude distribution plays a crucial role in enhancing the performance of marine radar. Due to variations in radar system parameters and oceanic environmental factors, sea clutter amplitude distribution exhibits multiple distribution types. Focusing solely on a single type of amplitude prediction lacks the necessary flexibility in practical applications. Therefore, based on the measured X-band radar sea clutter data from Yantai, China in 2022, this paper proposes a multi-task one-dimensional convolutional neural network (MT1DCNN) and designs a dedicated input feature set for the joint prediction of the type and parameters of sea clutter amplitude distribution. The results indicate that the MT1DCNN model achieves an F1 score of 97.4% for classifying sea clutter amplitude distribution types under HH polarization and a root-mean-square error (RMSE) of 0.746 for amplitude distribution parameter prediction. Under VV polarization, the F1 score is 96.74% and the RMSE is 1.071. By learning the associations between sea clutter amplitude distribution types and parameters, the model's predictions become more accurate and reliable, providing significant technical support for maritime target detection.

Keywords: radar data; sea clutter amplitude distribution; multi-task learning; convolutional neural networks; joint prediction

Citation: Wang, L.; Ma, L.; Wu, T.; Wu, J.; Luo, X. Joint Prediction of Sea Clutter Amplitude Distribution Based on a One-Dimensional Convolutional Neural Network with Multi-Task Learning. *Remote Sens.* **2024**, *16*, 3891. https://doi.org/10.3390/rs16203891

Academic Editor: Martin Gade

Received: 7 August 2024
Revised: 14 October 2024
Accepted: 17 October 2024
Published: 19 October 2024

1. Introduction

Marine radar, as an essential tool in ocean remote sensing [1], plays a crucial role in the detection of sea surface targets. However, in complex marine environments, radar detection of targets is inevitably influenced by sea clutter, i.e., the backscattered echoes from the sea surface [2]. Sea clutter exhibits complex characteristics, such as non-Gaussian and non-stationary behaviors, which vary spatiotemporally with marine and meteorological conditions. These characteristics pose significant constraints on radar detection performance [3,4]. Therefore, understanding sea clutter properties is crucial for enhancing radar target detection capabilities within cluttered marine backgrounds [5].

Currently, a substantial body of research has accumulated on the characterization of sea clutter [6–9], with amplitude distribution being a particularly important characteristic. The accuracy of sea clutter amplitude distribution modeling has a great impact on radar target detection capability and the effectiveness of clutter processing techniques [10,11]. Amplitude distribution modeling involves model selection and parameter estimation. The Rayleigh distribution, an early statistical theory applied to radar sea clutter amplitude distribution modeling, is primarily suitable for low–medium-resolution radars. However, with increasing radar resolution, sea clutter's statistical distributions deviate from the Rayleigh model, exhibiting enhanced peaks and tails [12], which are particularly evident

at small grazing angles. Consequently, to improve the fit between statistical models and empirical data, multi-parameter distribution types have gradually been applied. These include the Log-normal distribution [13,14], Weibull distribution [15], K distribution [16,17], and Pareto distribution [18], as well as composite distributions such as KK distribution [19], WW distribution, and K+Rayleigh distribution [20]. By appropriately selecting and adjusting these distribution models and parameters, it is possible to accurately simulate and predict sea clutter characteristics under different sea conditions, thereby enhancing radar systems' performance and reliability.

In various radar and oceanic environmental conditions, sea clutter exhibits significant differences in amplitude distribution characteristics, including dynamic range and tailing behavior across different models. For a given type of amplitude distribution, common methods for the parameter estimation of sea clutter amplitude distribution include maximum likelihood estimation (MLE) [21,22], moment estimation [23], quantile estimation, and parameter estimation based on intelligent evolutionary algorithms. Maximum likelihood estimation is known for its high estimation accuracy but involves complex mathematical computations. For distributions like the K distribution and Pareto distribution, which require solving complex nonlinear equations, closed-form solutions may not be achievable [24,25]. Moment estimation, based on mathematical statistics, offers simpler estimation algorithms but requires a substantial number of sample values and tends to have lower estimation precision.

Traditional statistical methods typically require large sample sizes for single-instance estimation, hampering the real-time estimation of sea clutter model parameters. With the ongoing development of deep learning technology, many researchers are turning to deep neural networks for parameter estimation. For instance, Mezache et al. [26] used artificial neural networks (ANNs) to estimate the parameters of the RiIG distribution based on cumulative distribution function (CDF) regression curves derived from measured sea clutter data. Machado et al. [27] proposed a neural network estimation method more suitable for real clutter environments to estimate the shape parameters of the Weibull distribution in real time. Wang et al. [28] trained neural networks on histogram statistics and simulation data to achieve better results than traditional statistical methods in estimating the parameters of Log-normal and K distributions. Xue et al. [29] proposed a bipercentiles feedforward neural network (BP-FFNN-η) method and tackled the challenge of dynamic changes in outlier proportions using a multiple network structure (MBP-FFNN-η), achieving accurate shape parameter estimation for K-distributed sea clutter. This method's robustness and adaptability in handling continuously changing environments are particularly noteworthy, offering significant practical value for enhancing sea surface monitoring systems' performance. These studies typically assume a specific distribution for sea clutter and focus on estimating the parameters of amplitude distribution under that assumption.

However, under the influence of various factors (such as wave height, wind speed, etc.), the sea clutter amplitude distribution may deviate from the expected model, making it difficult to represent dynamic ocean clutter with a fixed distribution model [30,31]. Ma [32] predicted the optimal distribution types and corresponding parameters for four distributions based on artificial neural networks and radar echo simulation data. Hua et al. [33] proposed a deep learning model, SE-ResNet-UWL, which includes Rayleigh, Log-normal, Weibull, and K distributions. This model predicts the most suitable distribution type and parameters for each distribution based on radar and oceanic atmospheric parameters, achieving joint prediction in complex spatiotemporal scenarios. However, due to the limited information contained in the input features and the imbalance of samples, the predictive performance for Rayleigh and Weibull distributions is suboptimal. Since the Rayleigh distribution does not meet the requirements of modern high-resolution radar, we propose replacing it with the Pareto distribution. To maximize the utilization of radar information, we extracted features from radar echo data under various ocean conditions and predicted the optimal distribution type and its parameters using a multi-task one-dimensional (1D) convolutional neural network (CNN), referred to as MT1DCNN. This

study, based on measured X-band sea clutter data from Yantai in 2022 [34–36], achieved optimal distribution type and parameter predictions for statistical sea clutter distributions, including Pareto, Log-normal, Weibull, and K distributions. Specifically, this paper makes the following contributions:

1. In this paper, an evaluation criterion for fitting sea clutter amplitude distribution that places greater emphasis on fitting accuracy in the tail regions is proposed. Unlike traditional methods that rely on simulated data for training, we annotate measured sea clutter data with this criterion and compile them into a dataset suitable for deep learning.
2. Although histogram features can be adjusted by altering the number of intervals to obtain features of different lengths, relying solely on a single histogram feature makes it challenging to achieve highly accurate predictions of more complex sea clutter characteristics. Therefore, we introduce two long-sequence features along with supplementary features to more comprehensively describe sea clutter characteristics.
3. A novel multi-task one-dimensional convolutional neural network is proposed for jointly predicting sea clutter amplitude distribution types and their corresponding parameters. The features proposed are effectively utilized by this model, which achieves state-of-the-art performance on the measured dataset.

2. Related Work

2.1. Multi-Task Learning

Multi-task learning (MTL) differs from single-task learning by enhancing model performance through the simultaneous optimization of multiple related tasks' loss functions [37,38]. It leverages task interrelations to improve data understanding and information extraction [39], effectively preventing overfitting and promoting generalization capabilities [40]. In MTL practice, hard sharing and soft sharing are the most used deep neural network implementation strategies: hard sharing involves fixed sharing of lower-layer parameters while keeping the upper-layer parameters independent, thereby reducing the risk of overfitting; soft sharing uses regularization techniques to flexibly control the degree of parameter sharing, increasing the training flexibility [41,42]. The loss function comprehensively considers specific objectives of each task (such as cross-entropy or mean squared error) and adjusts different tasks' contributions to the total loss through weighting factors, ensuring balanced influence among tasks and enabling optimization for task uncertainties or loss scale differences [43]. Additionally, well-designed auxiliary tasks serve as a significant advantage of MTL, supplementing the learning of the main task, introducing additional information resources, and improving the model's generalization and stability. The key lies in maintaining a delicate balance between task interrelations and complexity [44].

In this study, the application of MTL is not limited to theoretical discussion but is closely integrated with the practical needs of predicting sea clutter amplitude distributions. Our designed multi-task model not only predicts the type of sea clutter amplitude distribution but also simultaneously estimates the corresponding parameters (such as shape and scale parameters). These two tasks are closely related and jointly influence the understanding and processing of sea clutter signals. Through the hard sharing mechanism, the model's lower-layer parameters are shared between the classification task of predicting distribution types and the regression task of predicting corresponding distribution parameters, while the upper-layer parameters are adjusted according to the task characteristics. This ensures that the model can capture common features among tasks while handling task-specific differences.

2.2. One-Dimensional Convolutional Neural Network

Convolution, as a mathematical operation, is utilized in the field of deep learning through CNNs to efficiently extract features from data such as images and speech, performing tasks like classification and detection [45,46]. One-dimensional (1D) convolution is particularly suitable for analyzing long-sequence data, such as time series or text. It

captures features by sliding and weighting a 1D convolutional kernel over the sequence, and its flexibility lies in the ability to adjust the kernel size to fit different data lengths, reducing the number of parameters and simplifying computation [47], while retaining the ability to capture long-range dependencies. The unique advantages of 1D convolution have shown excellent performance in various fields, including natural language processing, time-series prediction, and bioinformatics [48], such as text classification, sentiment analysis, and gene sequence analysis, effectively integrating local features with contextual information to enhance model performance across various sequence tasks [49].

Considering the unique advantages of 1D CNNs in handling time-series data and the fact that sea clutter amplitude distribution is essentially composed of sequential signals, this study employs a 1D CNN for predicting sea clutter amplitude distribution. Addressing the diversity and dynamics of sea clutter, the 1D CNN can effectively capture the spatiotemporal features in sea clutter data through specialized convolutional kernel sizes and structures.

3. Methodology

In this section, we provide a detailed explanation of the method for joint prediction of amplitude distribution characteristics using multi-task learning combined with a 1D convolutional network. First, we introduce the multiple input data features of the sea clutter amplitude prediction model. Subsequently, we present the criteria for the optimal fitting distribution, aimed at determining the most suitable amplitude distribution type for sea clutter data. Finally, we describe the comprehensive design of the MT1DCNN architecture and its key implementation details.

3.1. Description of Multiple Sea Clutter Input Features

In complex and variable marine environments, the mapping relationship between radar data and sea clutter amplitude distribution characteristics is challenging to articulate clearly through mathematical or statistical theories [33]. Each radar dataset contains a vast number of values, and the correlation between values at individual positions and the final estimated parameters is low, making it difficult to intuitively reveal deeper information. Moreover, raw data often include low-quality samples [28]. Directly applying neural networks to fit the raw dataset results in poor performance due to the network's large scale, which is challenging to optimize and requires substantial computational resources. Therefore, preprocessing to optimize input features becomes crucial for enhancing model performance.

In this paper, three long-sequence features are extracted from the sea clutter data: histograms, the probability density function (PDF), and the complementary cumulative distribution function (CCDF). Additionally, ten fundamental sea clutter amplitude statistical measures are incorporated to enhance the feature set.

3.1.1. The Histogram Feature of Sea Clutter

In radar data processing, histogram analysis is a fundamental and effective method. It involves grouping continuous radar echo intensities or other feature values into specific intervals and then counting the number of data points within each interval. This method helps to visually display the distribution characteristics of data, captures the overall shape and local patterns of data, and is the basis for understanding the amplitude distribution types of sea clutter. For example, if the histogram shows clear peaks, it may indicate the presence of a dominant range of clutter intensity, while a broad and flat distribution indicates significant changes in clutter intensity. Therefore, histogram features help the model quickly capture the basic contour of amplitude distribution. However, if the interval size is too large, it may result in a large amount of data being clustered in the same group, reducing the model's accuracy. Conversely, if the interval size is too small, some groups may contain no data, thus diminishing the neural network's fitting effectiveness [28]. We

chose to set the number of bins to 100 to better retain the information inherent in the original data.

3.1.2. The PDF Feature of Sea Clutter

The PDF represents the probability density of sea clutter amplitude data within a given interval, i.e., the relative frequency of data points within each interval. It is computed using histogram data while considering the original data range. The calculation formula is as follows:

$$Xpdf_i = \frac{NN_i/N}{\Delta x}, \tag{1}$$

where NN_i is the frequency of the *i*-th interval in the sea clutter amplitude histogram, N is the total number of sea clutter amplitude data points, and Δx is the length of each interval. In the joint prediction model for sea clutter amplitude, using the PDF feature helps to accurately measure the probability of different amplitude values, making it easier to match statistical distribution models like the Log-normal and Weibull models.

3.1.3. The CCDF Feature of Sea Clutter

The CDF represents the cumulative probability of sea clutter amplitude data points being less than or equal to a given value, showing the cumulative distribution of the data from the minimum to the maximum values. The calculation formula is as follows:

$$Xcdf_i = \frac{\sum_{j=1}^{i} \mathrm{NN}_j}{N}, \tag{2}$$

where NN_j is the frequency of the *j*-th interval in the sea clutter amplitude histogram data. The CDF feature is helpful for analyzing the overall distribution of data and cumulative probabilities. However, in subsequent model training processes, the complement of the CDF, known as the CCDF, was used, which can be expressed by the following formula:

$$Xccdf_i = 1 - Xcdf_i, \tag{3}$$

which means that we focus on the cumulative probability of sea clutter amplitude data points exceeding a certain threshold. By using the CCDF, we can better capture the tail behavior and extreme values of the data (such as strong sea clutter), thereby enhancing the robustness and generalization ability of the model.

Although the PDF and CCDF features are both derived from histogram features, they each describe distinct levels of information. This ensures that the model can grasp the overall shape of the amplitude distribution on a macro level, while also capturing the detailed characteristics of the probability distribution. Additionally, it effectively handles extreme cases, enabling the joint prediction of the type and parameters of sea clutter amplitude distribution in complex oceanic environments.

3.1.4. Statistical Features of the Amplitude Distribution of Sea Clutter

To achieve higher predictive performance, sea clutter amplitude statistical measures were proposed that describe properties related to the location, dispersion, and distribution shape of the sea clutter amplitude data, comprising minimum (Min) and maximum (Max) values to identify extremes, variance (Var) and standard deviation (Sd) to quantify variability, and skewness (Skew) and kurtosis (Kurt) to characterize distribution shape, along with four quantiles representing data distribution at the 25th percentile (P25), 50th percentile (P50), 75th percentile (P75), and 90th percentile (P90). The formulae are as follows:

$$Xvar = \frac{1}{n}\sum_{i=1}^{n}\left(x_i - \bar{x}\right)^2, \tag{4}$$

$$Xsd = \&\sqrt{Xvar}, \tag{5}$$

$$Xskew = \frac{\frac{1}{n}\sum_{i=1}^{n}\left(x_i - \bar{x}\right)^3}{\left(\frac{1}{n}\sum_{i=1}^{n}\left(x_i - \bar{x}\right)^2\right)^{\frac{3}{2}}}, \tag{6}$$

$$Xkurt = \frac{\frac{1}{n}\sum_{i=1}^{n}\left(x_i - \bar{x}\right)^4}{\left(\frac{1}{n}\sum_{i=1}^{n}\left(x_i - \bar{x}\right)^2\right)^{2}} - 3, \tag{7}$$

where X_{var} represents the sea clutter amplitude variance, X_{sd} represents the standard deviation, S_{skew} represents the skewness, X_{kurt} represents the kurtosis, n is the sample size, x_i is the i-th sample point, and $\bar{x}$ is the sample mean.

Quantiles divide data into equally sized portions based on their order. The p-th percentile is a value in the dataset such that at least p percent of the observations are less than or equal to this value and at least $(1 - p)$ percent are greater than or equal to this value, where $0 < p < 1$.

They aid in understanding the central tendency, dispersion, and skewness of the sea clutter amplitude data, commonly used in data analysis and modeling.

3.2. Optimal Amplitude Distribution Annotation of Sea Clutter Based on TEIC Testing

In this study, Log-normal, Weibull, K, and Pareto distributions were selected as foundational statistical models. The parameters of the amplitude distribution were estimated using the MLE method. To determine the best-fitting model for the given sea clutter amplitude data, it is necessary to define a statistical metric that reflects the degree of fit between the statistical model and the data. This involves the issue of goodness-of-fit testing in statistical hypothesis testing. Traditional tests include the Kolmogorov–Smirnov (K-S) test, Cramer–Von Mises (CV) distance [50], chi-squared test [51], and statistical metrics like the D-statistic, quadratic statistic Q_0, and likelihood ratio [52], among others. Given that radar target detection emphasizes the tail part of sea clutter, a tail-emphasized inspection criterion (TEIC) was designed to prioritize the tail behavior. The formula is as follows:

$$TEIC = \sum_{i=1}^{N}\{|p(x_i; v, b) - p(x_i)|\{p(x_i > 0.1)\} + 10^2|p(x_i; v, b) - p(x_i)|\{p(x_i \leq 0.1)\}\}, \tag{8}$$

where $p(x_i)$ represents the PDF of sea clutter amplitude, and $p(x_i; v, b)$ represents the PDF of the statistical sea clutter amplitude distribution model fitted based on a specific shape parameter v and scale parameter b. A smaller value of the TEIC indicates a better fit.

We employed TEIC testing and selected the distribution with the smallest TEIC value as the optimal sea clutter amplitude distribution statistical model. Sea clutter amplitude distribution type labels were one-hot encoded, while the distribution parameter labels represent the shape and scale parameters obtained from the MLE of the distribution. Details of the input and output parameters for the multi-task 1D CNN used for jointly predicting amplitude distribution types and parameters are provided in Table 1.

Table 1. Details of the MT1DCNN model's input and output parameters.

Inputs (310)	Long-sequence features (300)	Histogram PDF CCDF
	Supplementary statistical features (10)	Min, Max Var, Std Skew, Kurt Quantiles (P25, P50, P75, P90)
Outputs (6)	Labels of sea clutter amplitude distribution type (4)	Log-normal, Weibull, K, Pareto
	Labels of sea clutter amplitude distribution parameter (2)	Shape parameter, scale parameter

3.3. Overview of the MT1DCNN Model

The overall structure of the MT1DCNN model for joint prediction of sea clutter amplitude distribution types and parameters is shown in Figure 1. This model leverages a 1D CNN to abstract and extract features from sea clutter amplitude histograms, PDFs, and CCDFs in a layer-by-layer manner. The three long-sequence features operate independently during this process, capturing key characteristics of the sea clutter signal from different perspectives without interference. This approach allows the model to extract richer and multi-layered feature representations from the sea clutter signals, thereby enhancing the ability to distinguish between different types of distributions and improving the accuracy of parameter predictions.

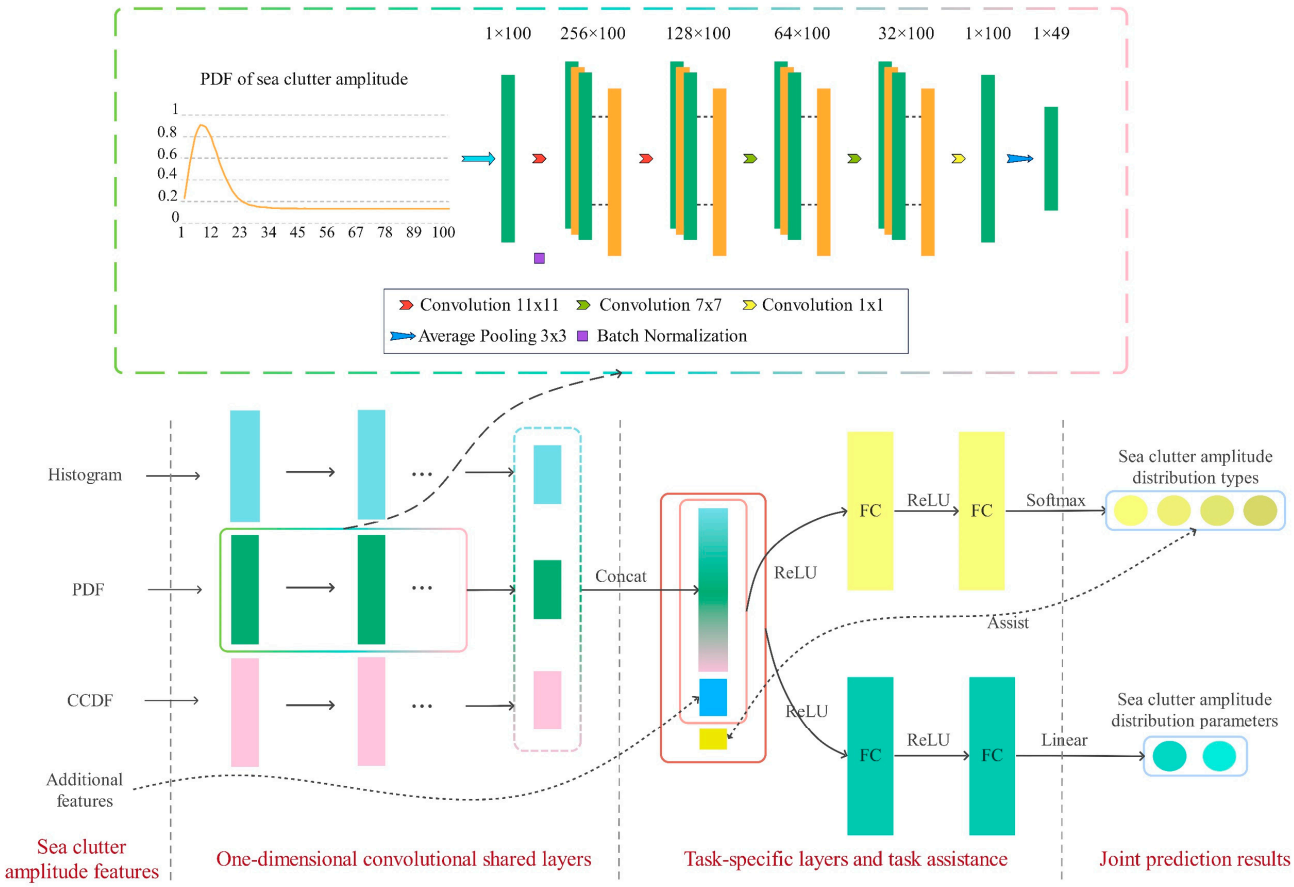

Figure 1. The architecture of MT1DCNN.

When extracting input features using a 1D CNN, taking the PDF feature as an example, the feature extraction network starts with a single-channel input and employs 256 large convolutional kernels, using padding to maintain the input size. The subsequent convolutional layers gradually reduce the number and size of the convolutional kernels while preserving the crucial spatial information. The final convolutional layer uses 1×1 convolutional kernels to reduce the dimensions to a single channel. Batch normalization is applied after specific convolutional layers to mitigate the vanishing gradient or exploding gradient problem, allowing better gradient propagation, enhancing the network stability, and improving training outcomes. This technique helps maintain the input distribution within a stable range, reducing the dependency on initial parameters and facilitating effective learning by the network. Subsequently, average pooling layers with a kernel size of 3 and a stride of 2 are used to downsample the feature maps, reducing the spatial dimensions of individual long-sequence features. This step significantly reduces the dimensionality of the features, making the resulting feature information more sensitive to background information and

increasing the receptive field, which can help improve the performance of the sea clutter amplitude distribution classification task.

In the task-specific layers and the task assistance module of MT1DCNN, all of the feature results processed by the 1D convolution are aggregated, forming a highly integrated and information-rich long-sequence feature representation. This joint feature is then integrated with supplementary statistical features, entering the private layers of the sea clutter amplitude distribution type classification and amplitude distribution parameter regression tasks. Specifically, the three types of long-sequence features undergo 1D convolution processing and are then concatenated into a joint feature with 147 dimensions, which is further integrated with 10 additional statistical features to form the input for the classification and regression task networks. The classification task receives an input with 157 dimensions (indicated by the light red box). Considering the close relationship between amplitude distribution type recognition and amplitude distribution parameter prediction, we also include the classification results in the regression task input, assigning them additional weights, and expand the input to 161 dimensions (indicated by the dark red box) to enhance the performance of the regression predictions. Both the classification and regression tasks have fully connected layers with 128 neurons, using the ReLU activation function consistent with the convolutional layers. The classification task employs a softmax layer to produce class probabilities, while the regression task directly outputs continuous predicted values.

The MT1DCNN model employs an MTL strategy, leveraging shared feature extraction layers to uncover key information common to sea clutter amplitude distribution type classification and amplitude distribution parameter regression tasks, encompassing the temporal patterns and nonlinear dynamic characteristics of the signal. Simultaneously, customized output layers for different tasks enhance the model's specialization in classification accuracy and parameter estimation. Notably, the positive interplay between tasks means that, when performing any specific task, the model can effectively utilize the feature knowledge extracted from other tasks, thereby improving its analysis and response capabilities in the complex sea clutter environment.

During the training process, stochastic gradient descent (SGD) was employed as the optimization algorithm, coupled with a constant decay strategy for the learning rate. These measures collectively ensured that the model could efficiently and rapidly converge to the optimal solution. For the choice of the loss function, the joint loss function proposed by Ma et al. [27] was adopted, specifically designed for the prediction of sea clutter amplitude distribution types and their parameters. The classification task used cross-entropy loss, while the regression task employed mean absolute error (MAE) as the loss calculation standard.

Additionally, Hua et al. [28] pointed out that predicting the shape and scale parameters of the K distribution might encounter issues where the parameters could take negative values. Based on this observation, they proposed a negative value suppression loss function specifically for the parameter prediction of the K distribution. In our training practice, we observed similar phenomena, such as the scale parameter of the Log-normal distribution occasionally taking negative values, the shape parameter of the Weibull distribution sometimes exceeding its upper limit of 2, and the scale parameter of the Pareto distribution potentially appearing negative. Based on these observations, a new range-constrained loss function was further designed and implemented, built upon the negative value suppression loss function, specifically optimized for the parameter prediction of these distributions. The overall loss function is as follows:

$$Loss = \lambda_1 MAELoss(v, \hat{v}) + \lambda_2 MAELoss\left(b, \hat{b}\right) + \lambda_3 CrossLoss(y, \hat{y}) + \lambda_4 RestrainLoss, \quad (9)$$

$$RestrainLoss = [L_l, L_w, L_k, L_p]Y, \quad (10)$$

$$L_l = ReLU(b), \quad (11)$$

$$L_w = ReLU(v - 2), \quad (12)$$

$$L_{k,p} = ReLU(-v) + ReLU(-b) \tag{13}$$

where $\lambda_1, \lambda_2, \lambda_3$ represent the weights of different losses, v and $\hat{v}$ refer to the predicted and target values of the shape parameter, respectively, while b and $\hat{b}$ represent the predicted and target values of the scale parameter, respectively. Additionally, y and $\hat{y}$ indicate the predicted and target values for the classification task, respectively. L_l, L_w, $L_{k,p}$ represent the range-constrained loss functions designed for the four distribution types, and Y is a 4×1 vector representing the one-hot encoded distribution type prediction results.

4. Experiments and Results

4.1. Measured Sea Clutter Data

The data used in this study originated from the Sea-Detecting Radar Data Sharing Program (SDRDSP) proposed by Liu et al. [34–36]. This dataset not only lays a solid foundation for the research but also significantly enhances transparency and collaboration in the field of ocean radar technology, holding important value for advancing progress in related areas. Specifically, this dataset includes experiments conducted using X-band solid-state fully polarimetric radar for sea surface detection. It contains target and sea clutter data under various sea conditions, resolutions, and grazing angle conditions. The sea conditions range from level 2 to level 5, corresponding to increasing and then decreasing wind and wave severity. The radar model used is the Tianao SPPR50P, with pulse widths ranging from 40 ns to 100 us and a transmit power of 100 W. It achieves a maximum range resolution of 6 m. The polarization modes include HH (1.8 m) and VV (2.4 m), and the antenna operates in both staring and circular scanning modes. It can perform a full 360° clockwise scan in the horizontal plane at speeds ranging from 2 to 48 revolutions per minute or operate in a staring mode at set angles. In this study, data from the staring mode were used, sampled at 60 MSPS (mega samples per second), corresponding to a sampling interval of 2.5 m. The overall temporal structure of a complete sampling is illustrated in Figure 2.

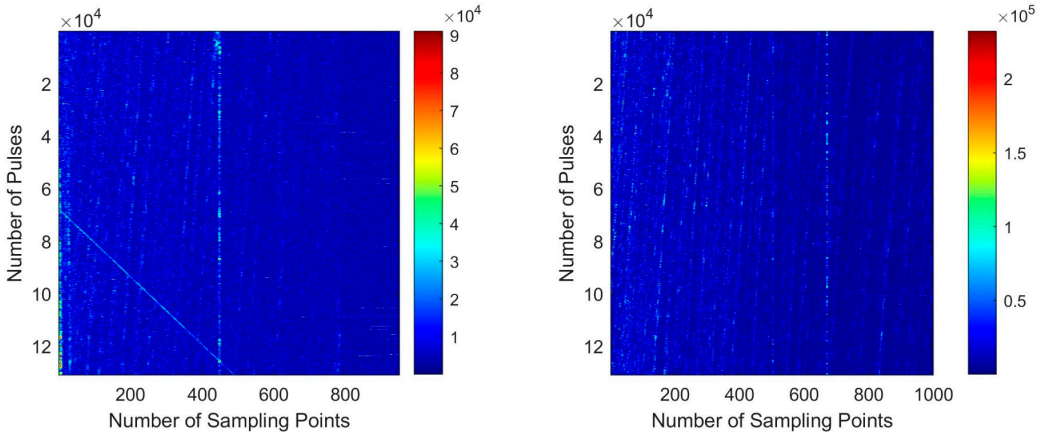

Figure 2. The overall temporal characteristics of T1 and T2 pulses: (**a**) T1 pulse echo (dB). (**b**) T2 plus Echo (dB).

The data include echoes from T1 pulses (single-carrier frequency transmission signals) and T2 pulses (LFM transmission signals). The distance dimension samples extracted from T1 pulse echoes number 950, and those from T2 pulse echoes number 1000 samples, totaling 131,072 pulses stored.

Because the data contain targets such as buoys and ships, their effects were removed to retain only clean sea clutter data for analysis.

After extracting and annotating features from the Yantai 2022 measured X-band sea clutter data, HH and VV polarization datasets suitable for joint prediction were obtained,

each containing approximately 135,000 samples. According to the TEIC, the optimal distributions for HH-polarized sea clutter were found to be 13.3% for Log-normal distribution, 18.4% for Weibull distribution, 5% for K distribution, and 63.3% for Pareto distribution. For VV polarization, these proportions were 6.2%, 18%, 22.9%, and 52.9%, respectively.

However, due to the approximate solutions provided by the MLE method used for K distribution and Pareto distribution, some shape parameter estimates were notably larger than expected. Figure 3 illustrates the data distribution of these shape parameters for both distribution types, with a maximum value limit set at 100 to focus on details in high-density regions. In HH-polarized sea clutter data, 0.6% of K distribution shape parameters exceeded 30, and 0.3% of Pareto distribution shape parameters exceeded 20. In VV polarization mode, these percentages were 0.5% and 4%, respectively.

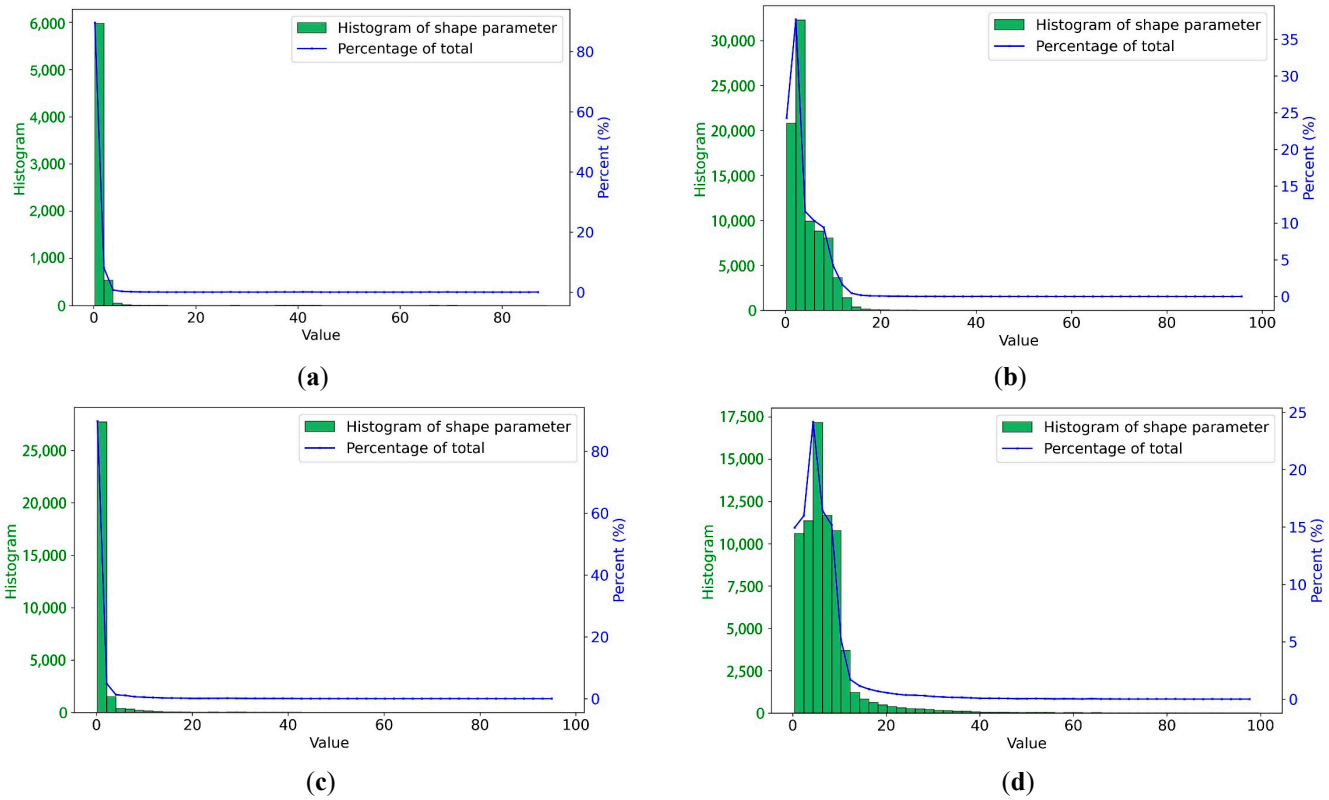

Figure 3. The data distribution of shape parameters for K and Pareto distributions: (**a**) K distribution of sea clutter in HH polarimetric radar. (**b**) Pareto distribution of sea clutter in HH polarimetric radar. (**c**) K distribution of sea clutter in VV polarimetric radar. (**d**) Pareto distribution of sea clutter in VV polarimetric radar.

Considering that these outliers in shape factors may adversely affect the training effectiveness of models, the decision was made to remove these anomalies to ensure high data quality and stability in subsequent model training. This decision was based on a comprehensive assessment of potential biases introduced by outliers and their potential impact on model performance. Our aim was to optimize the effectiveness and reliability of model training by accurately controlling the data quality.

As a result, a dataset of optimal amplitude distribution types and their corresponding parameters was obtained based on measured sea clutter data. The amplitude distribution dataset for sea clutter in HH polarization consisted of 133,938 data points, while the VV polarization data contained 128,759 data points. The dataset was divided into training, validation, and test sets at a split ratio of 70%:15%:15%. Tables 2 and 3 present detailed information about this dataset, including sample counts for each distribution, as well as ranges of the shape and scale parameters.

Table 2. Dataset details for sea clutter amplitude distribution in HH polarization radar.

Distribution Types	Range of Shape Parameter	Range of Scale Parameter	Number
Log-normal	[0.740, 1.205]	[−0.692, −0.245]	18,058
Weibull	[0.789, 2]	[0.671, 1.129]	24,016
K	[0.224, 29,652]	[0.074, 23.130]	6622
Pareto	[0.458, 17.710]	[0.821, 8.871]	85,241

Table 3. Dataset details for sea clutter amplitude distribution in VV polarization radar.

Distribution Types	Range of Shape Parameter	Range of Scale Parameter	Number
Log-normal	[0.121, 1.435]	[−0.989, −0.007]	8408
Weibull	[0.849, 2]	[0.807, 1.129]	21,223
K	[0.316, 20.378]	[0.154, 15.764]	30,719
Pareto	[0.587, 19.816]	[0.819, 3.416]	68,408

4.2. Evaluation Metrics for Sea Clutter Amplitude Distribution Type and Parameter Predictions

In binary classification problems, there are typically four types of classification outcomes: true positive (TP), true negative (TN), false positive (FP), and false negative (FN). These values are used to calculate the precision (Pre), recall (Rec), and F1 score. For the multi-class classification problem of sea clutter amplitude distribution types, it is common to decompose the problem into multiple binary classification tasks, treating each class as the positive class in turn while considering the rest as negative classes. Evaluation metrics are then averaged across these tasks, as formulated below:

$$\mathrm{Pre}_i = \frac{TP_i}{TP_i + FP_i}, \tag{14}$$

$$\mathrm{Rec}_i = \frac{TP_i}{TP_i + FN_i}, \tag{15}$$

$$F1_i = \frac{2 \times Pre_i \times Rec_i}{Pre_i + Rec_i}, \tag{16}$$

$$Weighted\ Avg\ F1 = \sum_{i=1}^{n} (F1_i \times \frac{s_i}{N}), \tag{17}$$

where i denotes the categories of amplitude distribution of sea clutter, n represents the number of classes, s_i denotes the number of samples in the i-th class, and N represents the total number of samples in the test set. A higher precision indicates fewer errors when the model predicts positive instances, reflecting the reliability of the model's predictions. Higher recall indicates the model's ability to better capture actual positive samples, demonstrating stronger classification capabilities in the task of classifying sea clutter amplitude distribution types. The F1 score is the harmonic mean of precision and recall, providing a comprehensive evaluation of the model's performance.

Given that our amplitude distribution classification task involves a four-class imbalance, as shown in Tables 2 and 3, the simple average F1 score might be dominated by classes with more samples, such as the Pareto distribution; thus, it may not accurately reflect the overall performance. By using weighted average F1 scores, the sample sizes in each class are accounted for, weighting the F1 scores of different classes to comprehensively assess the model's performance across all classes. Therefore, the weighted average F1 score was adopted as the metric to assess the overall classification performance of the model, with a higher score indicative of greater accuracy in predicting the distribution types of sea clutter.

In regression problems, common evaluation metrics include the mean absolute error (MAE), RMSE, and R-squared (R^2), with their mathematical formulations provided as follows:

$$MAE = \frac{1}{n}\sum_{i=1}^{n}|y_i - \hat{y}_i|, \tag{18}$$

$$RMSE = \sqrt{\frac{1}{n}\sum_{i=1}^{n}(y_i - \hat{y}_i)^2}, \tag{19}$$

$$R^2 = 1 - \frac{\sum_{i=1}^{n}(y_i - \hat{y}_i)^2}{\sum_{i=1}^{n}\left(y_i - \bar{y}\right)^2}, \tag{20}$$

where y_i represents the true values, i.e., the sea clutter amplitude distribution parameters in the test set, $\hat{y}_i$ represents the predicted values, $\bar{y}$ is the mean of the true values, and n is the number of samples. The R^2 score indicates the degree to which the model fits the data, with values ranging from 0 to 1; a value closer to 1 indicates a better model fit. Since the model has two regression output values, these metrics are calculated for each output variable, and the average is taken as the evaluation metric for the overall regression performance of the model.

4.3. Analysis of Sea Clutter Amplitude Distribution Type and Parameter Predictions Based on MT1DCNN

The MT1DCNN model proposed in this study efficiently predicted the amplitude distribution types of sea clutter under complex sea conditions and their corresponding parameters, with specific results illustrated in Figure 4.

Figure 4a,b depict the confusion matrix heatmaps of the sea clutter amplitude distribution classification task under HH and VV polarization, respectively. Class 3 represents the Pareto distribution, class 2 represents the K distribution, class 1 represents the Weibull distribution, and class 0 represents the Log-normal distribution. Taking the correct identification of HH-polarized sea clutter samples following the Pareto distribution as an example, the percentage on the right of the cell indicates a precision of 98.85%, the percentage at the bottom indicates a recall of 98.59%, the middle number indicates a count of 12,643 sea clutter samples, and the percentage below the number represents its proportion in the total test samples, at 62.93%. Although the data of HH-polarized sea clutter K distribution are sparse, accounting for less than 5%, they still perform well in the classification task, with a precision of 88.42%. Pareto distribution data are the most abundant and show the best performance, with precision exceeding 95% for the other distributions as well. In VV polarization mode, with an increase in K distribution data, the classification precision significantly improves to 96.26%, while the Pareto distribution continues to perform the best with a precision of 97.57%, and the precision for the other distributions remains around 95%.

Figure 4c,d show scatter density plots of the sea clutter amplitude distribution shape parameter prediction results under HH and VV polarization, respectively. The horizontal axis represents the amplitude distribution shape parameters on the test set, and the vertical axis represents the values predicted by the MT1DCNN model. The shape parameters of the four distributions are mainly concentrated between 0 and 3, with only a few data points from the K and Pareto distributions exceeding this range, and the data density decreases with increasing values. Additionally, although VV polarization mode has more data points with shape parameter values exceeding 3 compared to HH polarization, resulting in a slightly higher MAE of 0.09 and RMSE of 0.359, the R^2 values remain relatively close and at a high level. Figure 4e,f display the results of the scale parameter predictions. The R^2 value for the scale parameter of the sea clutter amplitude distribution predicted by the MT1DCNN model in HH polarization mode reaches 0.796, while for VV polarization the R^2 value for the scale parameter is 0.658.

Overall, the MT1DCNN model demonstrates reliable performance in predicting both amplitude distribution types and corresponding parameters under various sea conditions.

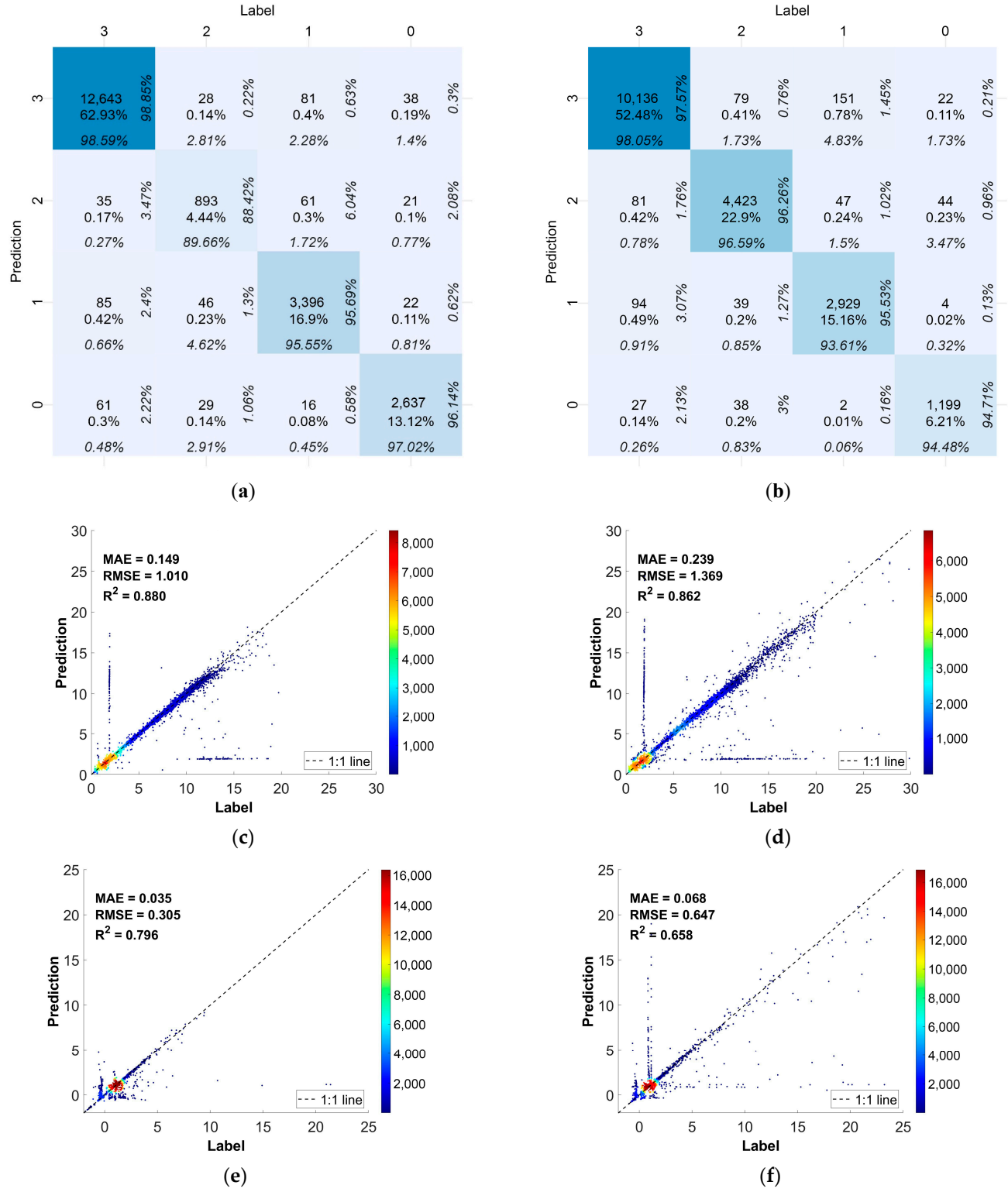

Figure 4. Sea clutter amplitude distribution joint prediction results of the MT1DCNN model are presented as follows: for the classification task, outcomes are depicted via a confusion matrix heatmap, whereas the regression task results are illustrated using scatter density plots. (**a**) Amplitude distribution types of HH polarization. (**b**) Amplitude distribution types of VV polarization. (**c**) Shape parameter of HH polarization. (**d**) Shape parameter of VV polarization. (**e**) Scale parameter of HH polarization. (**f**) Scale parameter of VV polarization.

4.4. Ablation Analysis and Impact Study of Input Features in the MT1DCNN Model

To improve the prediction accuracy, the method designed in this study integrates multiple features. We conducted a series of ablation experiments to thoroughly investigate the specific impact of each feature on the overall prediction performance. The experimental results are detailed in Tables 4 and 5 where AS represents the amplitude statistical features.

Table 4. The influence of different features on the predictive performance of MT1DCNN under HH polarization.

Features	F1 Score	MAE	RMSE	R^2
Histogram	95.75%	0.194	1.119	0.811
PDF	95.33%	0.207	1.178	0.801
CCDF	96.65%	0.125	0.811	0.863
Histogram + AS	96.67%	0.124	0.721	0.878
Histogram + PDF	95.79%	0.178	1.112	0.812
Histogram + PDF + CCDF	97.03%	0.109	0.723	0.878
Histogram + PDF + CCDF + AS	97.40%	0.092	0.746	0.906

Table 5. The influence of different features on the predictive performance of MT1DCNN under VV polarization.

Features	F1 Score	MAE	RMSE	R^2
Histogram	95.99%	0.236	1.327	0.863
PDF	95.83%	0.243	1.347	0.861
CCDF	95.98%	0.185	1.272	0.868
Histogram + AS	95.87%	0.185	1.284	0.867
Histogram + PDF	95.96%	0.235	1.305	0.865
Histogram + PDF + CCDF	96.15%	0.177	1.281	0.868
Histogram + PDF + CCDF + AS	96.74%	0.154	1.071	0.881

The results indicate that, among long-sequence features, the CCDF has the greatest impact, particularly in the prediction of sea clutter amplitude distribution parameters, where it shows a clear advantage. Additionally, the performance of the CCDF is comparable to that of histograms + AS. Under VV polarization, AS does not significantly improve the accuracy of predicting sea clutter amplitude distribution types, but it has a more pronounced effect on the distribution parameters. As the number of features increases, the prediction accuracy of the model improves, but the computational cost also increases. Specifically, the test sets for HH polarization and VV polarization contain 20,090 and 19,313 data points, respectively. When all features are used as network inputs, the corresponding testing times are 0.46 s and 0.44 s, respectively.

4.5. Comparative Analysis of Sea Clutter Amplitude Distribution Type and Parameter Prediction Results

4.5.1. Comparative Analysis of the Prediction Results of the MT1DCNN Model and the Traditional Method

In the process of estimating the parameters of the actual sea clutter amplitude distribution and using these parameters as dataset labels, we employed the MLE method. The predictive performance of MT1DCNN is directly influenced by the parameter estimation methods used to generate the training dataset. As shown in Figure 5, MT1DCNN not only achieves overall performance comparable to that of MLE but also slightly outperforms MLE in fitting the tails of certain data distributions. We randomly selected two sets of data for further analysis, and the results are shown in Figure 6. Under the same distribution, MT1DCNN provides more accurate predictions for the tail regions, and after extensive training it can adaptively select the most suitable distribution type based on the actual data.

Although this deviates from the labels that we artificially set, it is more in line with the actual situation.

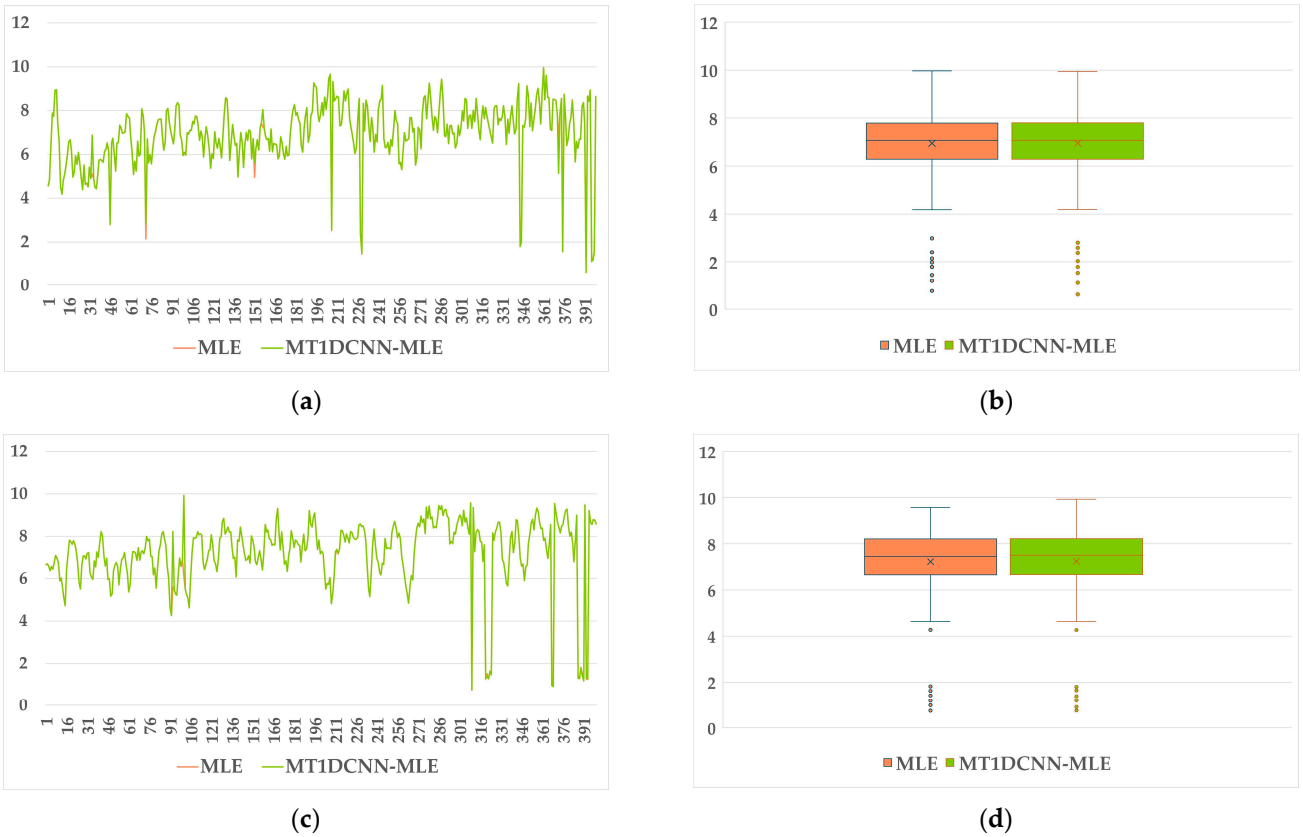

Figure 5. TEIC comparison of two methods: MLE, and MT1DCNN based on MLE. (**a**) TEIC value comparison under HH polarization. (**b**) Boxplot of TEIC values under HH polarization. (**c**) TEIC value comparison under VV polarization. (**d**) Boxplot of TEIC values under VV polarization.

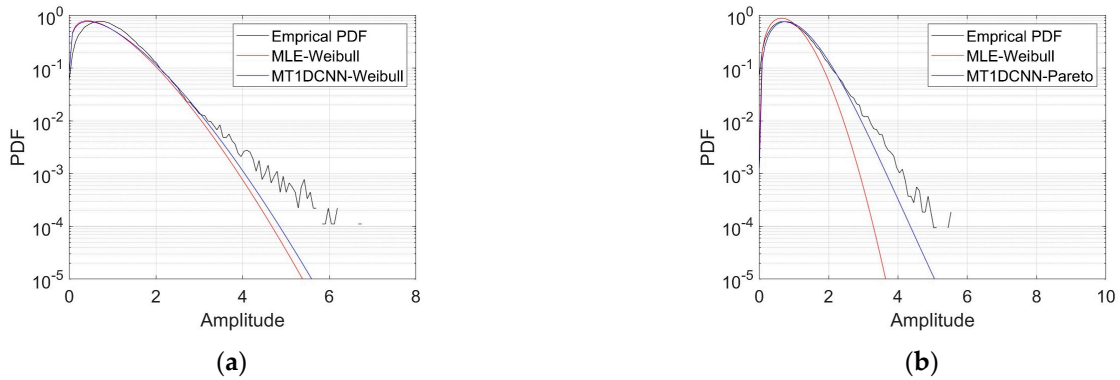

Figure 6. Comparison of results for predicting the real sea clutter amplitude distribution using different parameter estimation methods: (**a**) Prediction results under HH polarization. (**b**) Prediction results under VV polarization.

4.5.2. Comparative Analysis of the Prediction Results of the MT1DCNN Model and Other Deep Learning Models

To assess the effectiveness of MT1DCNN, we improved the fully connected artificial neural network proposed by Ma [27] by increasing the number of hidden layers and neurons to accommodate more complex data, termed the baseline model (DNN7), and compared it with our proposed method. DNN7 consists of seven hidden layers, each containing

128 neurons, with parameter sharing in five of the hidden layers, and with the input limited to histogram features. To evaluate the role of additional long-sequence and supplementary features, we augmented DNN7 with these features and adjusted the network structure, resulting in DNN7-AF. The number of hidden layers remained unchanged, but the number of neurons in the first three layers was increased. To study the impact of task assistance, we removed the task assistance module from MT1DCNN, denoted as MT1DCNN-NT.

The above models were trained using the same sea clutter dataset. Figure 7 illustrates the F1 scores and loss variation curves on the validation set for the four models under HH-polarized sea clutter, while Figure 8 shows the results for VV-polarized sea clutter. Additionally, Table 6 presents the F1 scores and various regression metrics on the test set under HH polarization, and Table 7 provides the corresponding results for VV polarization. Combined with Tables 6 and 7, it can be observed that our proposed new features exhibit significant improvements compared to the single histogram feature, in both HH and VV polarization.

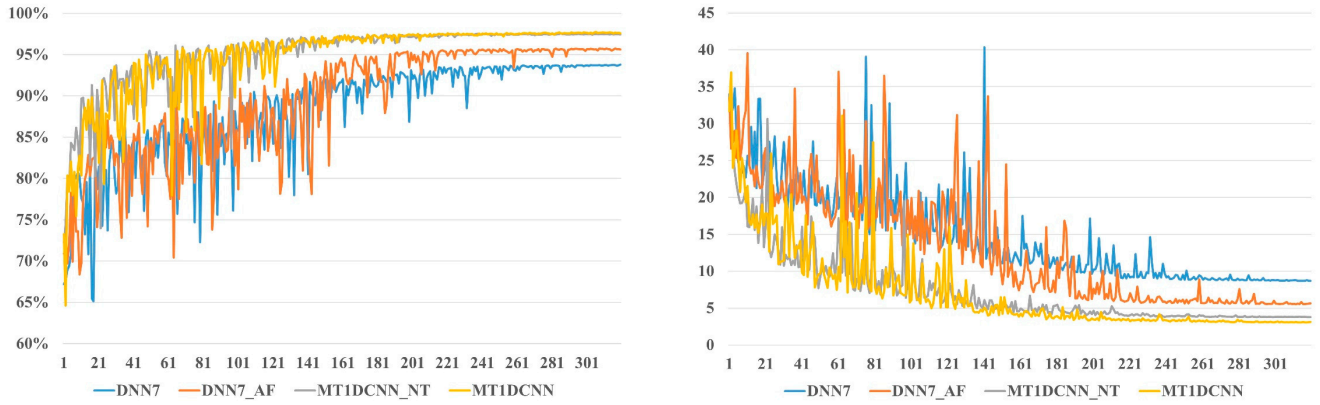

(**a**) (**b**)

Figure 7. Comparison of training results of different models and epochs on the HH polarization sea clutter validation set: (**a**) F1 score. (**b**) Validation loss.

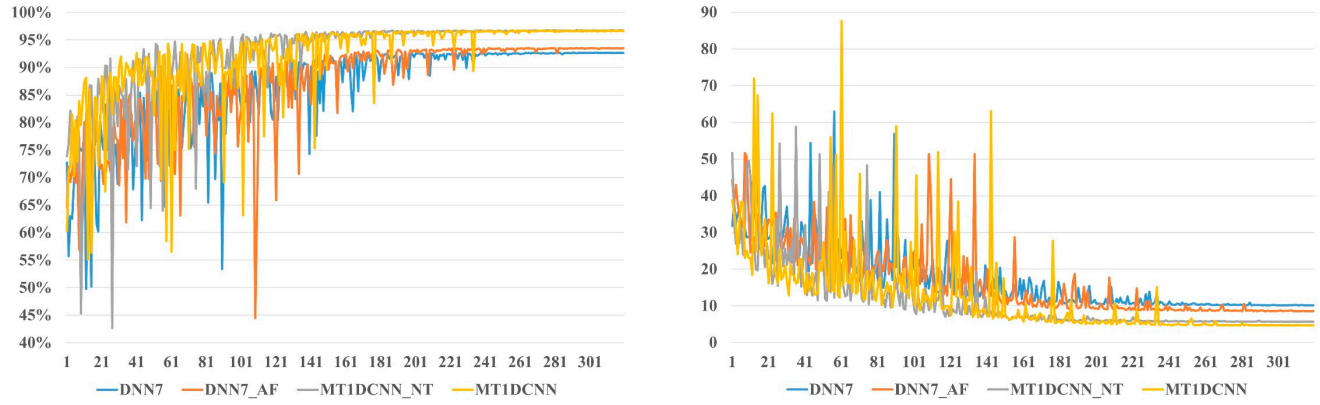

(**a**) (**b**)

Figure 8. Comparison of training results of different models and epochs on the VV polarization sea clutter validation set: (**a**) F1 score. (**b**) Validation loss.

Table 6. Prediction results for sea clutter amplitude distribution in HH polarization radar across different models.

Models	F1 Score	MAE	RMSE	R^2
DNN7	93.65%	0.269	1.125	0.786
DNN-AF	95.64%	0.169	0.855	0.876
MT1DCNN-NT	97.33%	0.121	0.765	0.901
MT1DCNN	97.40%	0.092	0.746	0.906

Table 7. Prediction results for sea clutter amplitude distribution in VV polarization radar across different models.

Models	F1 Score	MAE	RMSE	R^2
DNN7	92.81%	0.329	1.354	0.810
DNN-AF	93.50%	0.277	1.291	0.828
MT1DCNN-NT	96.88%	0.202	1.174	0.857
MT1DCNN	96.74%	0.154	1.071	0.881

The sea clutter amplitude distribution joint prediction performance of DNN7-AF is superior to that of DNN7. Specifically, the F1 scores for amplitude distribution classification tasks improved by 1.99% and 0.69%, respectively, and the R^2 values for parameter prediction tasks increased by 0.09 and 0.018, respectively. MT1DCNN-NT showed F1 scores very close to those of MT1DCNN, but the latter demonstrated more pronounced advantages in parameter prediction tasks.

Due to the heavy-tailed characteristics of K distribution and Pareto distribution, their parameters can simulate each other within a certain range, making them more difficult to distinguish in classification compared to other distribution types. In the VV polarization dataset, the proportion of K distribution to Pareto distribution is approximately 5.8 times higher than in the HH polarization dataset, indicating higher classification difficulty in VV polarization. Therefore, under the same model conditions, HH polarization consistently outperforms VV polarization in all performance metrics. However, MT1DCNN-NT significantly reduces this gap, reducing the F1 score difference between HH and VV polarization from about 2% to about 0.5% compared to DNN7-AF.

Tables 8 and 9 provide a more detailed display of the F1 scores for the four distribution types across different models. In HH polarization mode, K distribution data are sparse, resulting in consistently lower F1 scores compared to other distributions. In VV polarization mode, despite the K distribution having more data than the Log-normal and Weibull distributions, the F1 scores of the DNN7 and DNN-AF models for K distribution remain the lowest. However, our proposed 1D CNN provides a deeper understanding of the characteristics of the four distributions. The F1 score for HH-polarized sea clutter K distribution improved by approximately 10%, a significant increase compared to other distributions. In VV polarization mode, this metric increased by about 6%, surpassing both the Log-normal and Weibull distributions, with the distribution with the fewest data (Log-normal distribution) also showing a considerable improvement.

Table 8. Comparison of F1 scores across various models for each distribution under HH polarization.

Models	Log-Normal	Weibull	K	Pareto
DNN7	93.42%	88.88%	78.17%	96.23%
DNN-AF	94.35%	93.61%	79.72%	97.72%
MT1DCNN-NT	96.31%	95.36%	90.02%	98.67%
MT1DCNN	96.57%	95.62%	89.03%	98.72%

Table 9. Comparison of F1 scores across various models for each distribution under VV polarization.

Models	Log-Normal	Weibull	K	Pareto
DNN7	90.26%	91.62%	89.73%	94.84%
DNN-AF	91.63%	92.70%	90.45%	95.33%
MT1DCNN-NT	95.23%	94.90%	96.40%	97.89%
MT1DCNN	94.59%	94.56%	96.42%	97.81%

These results indicate that, compared to fully connected networks, 1D CNNs can more effectively extract information from long-sequence features, even in the presence of imbalanced samples, thereby learning deeper differences between different distributions.

Furthermore, task assistance also plays a crucial role. Despite MT1DCNN not achieving the highest F1 score on the VV polarization test set, as observed from Figures 7 and 8, after basic model training, MT1DCNN and MT1DCN-NT showed comparable performance in classification tasks, suggesting that they reach similar levels. However, in parameter prediction tasks, MT1DCNN consistently outperforms MT1DCN-NT, with an increase in MAE of approximately 0.03 for HH polarization radar sea clutter amplitude distribution parameters, and approximately 0.05 for VV polarization. To further investigate the specific performance of task assistance, these two parameters were separately analyzed, as shown in Tables 10 and 11.

Table 10. Comparison of sea clutter amplitude distribution parameter prediction performance among models under HH polarization.

Parameters	Models	MAE	RMSE	R^2
Shape	DNN7	0.468	1.551	0.714
	DNN7-AF	0.280	1.161	0.840
	MT1DCNN-NT	0.188	1.032	0.873
	MT1DCNN	0.149	1.010	0.880
Scale	DNN7	0.069	0.350	0.729
	DNN7-AF	0.057	0.340	0.745
	MT1DCNN-NT	0.053	0.322	0.771
	MT1DCNN	0.035	0.305	0.796

Table 11. Comparison of sea clutter amplitude distribution parameter prediction performance among models under VV polarization.

Parameters	Models	MAE	RMSE	R^2
Shape	DNN7	0.515	1.645	0.796
	DNN7-AF	0.418	1.544	0.821
	MT1DCNN-NT	0.272	1.337	0.865
	MT1DCNN	0.239	1.369	0.862
Scale	DNN7	0.144	0.979	0.200
	DNN7-AF	0.135	0.973	0.211
	MT1DCNN-NT	0.132	0.985	0.192
	MT1DCNN	0.068	0.647	0.658

As the sea clutter amplitude characteristics vary, the shape parameters of the K distribution and Pareto distribution exhibit consistent trends, while their scale parameters show opposite trends. Specifically, the shape parameter of the K distribution increases alongside its scale parameter, indicating a certain linear relationship between them. In contrast, the scale parameter of the Pareto distribution decreases as the shape parameter increases, with the reduction rate gradually diminishing, demonstrating a nonlinear relationship.

Therefore, predicting parameters for both the K distribution and Pareto distribution poses significant challenges. This is also why, as shown in Table 11, the prediction perfor-

mance of scale parameters in the VV-polarized sea clutter amplitude parameter prediction task is relatively poorer. Under these challenging conditions, compared to other models, MT1DCNN achieves an approximately 0.45 increase in R^2 value for scale parameter prediction, representing an improvement of more than 200%. This underscores the significant role of task assistance methods in enhancing the accuracy of scale parameter predictions, while improvements in shape parameter predictions are equally notable.

5. Discussion

This study departed from the traditional method of obtaining experimental data from simulated data and instead extracted a dataset for training purposes from actual radar measurement data. Despite its similarity to real-world scenarios, this approach faces several imbalances among the collected data samples: firstly, there is an imbalance in the quantities of samples among the four distribution types; secondly, even within the same distribution type, the density of parameter values varies across different ranges. Furthermore, although the MLE method offers high accuracy in parameter estimation, it involves significant computational complexity and does not yield closed-form solutions when dealing with K distribution and Pareto distribution.

In Section 4.1, a crucial measure was implemented by setting upper limits on the shape parameters of the K distribution and Pareto distribution. This decision was motivated by concerns that outliers could potentially bias the model training. The effectiveness of this measure was evident in subsequent analyses, as particularly highlighted in Table 11, where the MT1DCNN model achieved the lowest MAE of 0.239 for predicting VV-polarized sea clutter amplitude shape parameters compared to other models, albeit with slightly higher RMSE than the MT1DCNN-NT model. This discrepancy arises because RMSE is more sensitive to extreme errors, whereas MAE remains relatively robust and is less affected by individual extreme values. This phenomenon aligns with the higher data density observed in Figure 3d for VV-polarized sea clutter Pareto distribution shape parameters in the higher numerical range.

In real marine environments, variations in sea clutter amplitude characteristics are primarily concentrated within lower ranges of shape parameters. Even slight adjustments in these parameters within this range can significantly alter the probability density distribution of sea clutter amplitudes. Conversely, as shape parameters increase to higher numerical ranges, such as in the K and Pareto distributions, significant fluctuations in shape parameters yield relatively moderate changes in the probability density distribution of sea clutter amplitudes, indicating a weakened influence of shape parameter changes within this range. Therefore, a model capable of providing more accurate predictions in regions with smaller shape parameters is particularly important. Although the MT1DCNN's predictions in the higher value range may not be as precise as in the lower value range (as reflected by a higher RMSE), in the region where the characteristics of sea clutter amplitude vary the most actively—namely, the region with lower shape parameters—the MT1DCNN demonstrates its position as the optimal model with the lowest MAE. This also reflects the robust predictive capability of the MT1DCNN model when handling complex data.

In future work, we plan to adopt a more targeted approach by selecting the optimal parameter estimation method for each specific distribution, rather than relying on a single method. Additionally, we aim to reduce the number of parameters while refining them to maintain the model's prediction accuracy and enhance the real-time performance of the radar system.

6. Conclusions

In this study, a series of features, including the PDF, CCDF, and several statistical features, were extracted from the raw sea clutter data for the prediction of sea clutter amplitude distribution types and parameters. Additionally, a new criterion, the TEIC, was proposed to discriminate the optimal fitting distribution of sea clutter. Based on this criterion, actual sea clutter data were annotated for training deep learning networks. The

MT1DCNN model was also introduced to jointly predict the types of sea clutter amplitude distributions (Log-normal, Weibull, K, and Pareto distribution) and their corresponding parameters (shape and scale parameters). Furthermore, considering that the description of sea clutter amplitude distribution characteristics depends on both distribution type and parameters, a task assistance mechanism was utilized to transfer the results of the classification tasks to the parameter prediction tasks for more accurate prediction of amplitude distribution parameters. The experimental results show that the prediction accuracy of sea clutter amplitude distribution types and parameters under HH and VV polarization was improved to some extent. Compared to the baseline method, the F1 score for the HH polarization radar sea clutter amplitude distribution type increased by 3.75%, and the RMSE decreased by 0.379; the F1 score under VV polarization increased by 3.93%, and the RMSE decreased by 0.283. These results indicate that this method exhibits optimal performance in predicting sea clutter amplitude characteristics under complex marine conditions, providing technical support for radar target detection. In the future, integrating data from different periods and regions, or combining radar data with other types of remote sensing data, such as optical satellite images and SAR images, could further enhance the classification accuracy and expand the application scope of this method.

Author Contributions: Conceptualization, L.M., J.W. and L.W.; methodology, L.W. and X.L.; software, L.W.; validation, L.W., L.M., T.W., J.W. and X.L.; formal analysis, L.W. and J.W.; investigation, L.W. and X.L.; resources, L.M. and T.W.; data curation, L.M. and T.W.; writing—original draft preparation, L.W.; writing—review and editing, L.M.; visualization, L.W.; supervision, L.M.; project administration, L.M.; funding acquisition, L.M. and T.W. All authors have read and agreed to the published version of the manuscript.

Funding: This research was funded by the National Natural Science Foundation of China (Grants No. 62101297 and 62271381).

Data Availability Statement: Data are contained within the article.

Acknowledgments: We express our gratitude to Liu Ningbo and his team from the Naval Aviation University for providing the measured X-band sea clutter data published in the Journal of Radars.

Conflicts of Interest: Author Xiang Luo was employed by the company Wuhan Wisdom Bio-Technology Co., Ltd. The remaining authors declare that the research was conducted in the absence of any commercial or financial relationships that could be construed as a potential conflict of interest.

References

1. Amani, M.; Ghorbanian, A.; Asgarimehr, M.; Yekkehkhany, B.; Moghimi, A.; Jin, S.; Naboureh, A.; Mohseni, F.; Mahdavi, S.; Layegh, N.F. Remote Sensing Systems for Ocean: A Review (Part 1: Passive Systems). *IEEE J. Sel. Top. Appl. Earth Obs. Remote Sens.* **2022**, *15*, 210–234. [CrossRef]
2. Guo, L.; Wei, Y. Status and Prospects of Electromagnetic Scattering Echoes Simulation from Complex Dynamic Sea Surfaces and Targets. *J. Radars* **2023**, *12*, 76–109.
3. Xue, J.; Ma, M.; Liu, J.; Pan, M.; Xu, S.; Fang, J. Wald- and Rao-Based Detection for Maritime Radar Targets in Sea Clutter with Lognormal Texture. *IEEE Trans. Geosci. Remote Sens.* **2022**, *60*, 5119709. [CrossRef]
4. Xue, J.; Xu, S.; Liu, J. Persymmetric Detection of Radar Targets in Nonhomogeneous and Non-Gaussian Sea Clutter. *IEEE Trans. Geosci. Remote Sens.* **2022**, *60*, 5103709. [CrossRef]
5. Zhang, J.; Zhang, Y.; Xu, X.; Li, Q.; Wu, J. Estimation of Sea Clutter Inherent Doppler Spectrum from Shipborne S-Band Radar Sea Echo. *Chin. Phys. B* **2020**, *29*, 068402. [CrossRef]
6. Li, Y.; Ma, L.; Zhang, Y.; Wu, T.; Zhang, J.; Li, H. Prediction of Sea Surface Reflectivity under Different Sea Conditions Based on the Clustering of Marine Environmental Parameters. *Remote Sens.* **2023**, *15*, 5318. [CrossRef]
7. Yang, G.; Zhang, X.; Zou, P.; Shui, P. Compound-Gaussian Model with Nakagami-Distributed Textures for High-Resolution Sea Clutter at Medium/High Grazing Angles. *Remote Sens.* **2024**, *16*, 195. [CrossRef]
8. Wang, Q.; Qi, C.; Yan, J. A Facet-Based Model and Doppler Analysis for Bistatic Electromagnetic Scattering from 3-D Time-Evolving Sea Surface. *IEICE Electron. Express* **2024**, *21*, 20240001. [CrossRef]
9. Liao, X.; Xie, J.; Zhou, J. A Data-Driven Optimization Method for Simulating Arbitrarily Distributed and Spatial-Temporal Correlated Radar Sea Clutter. *IEEE Trans. Geosci. Remote Sens.* **2023**, *61*, 5110815. [CrossRef]
10. Shi, S.; Shui, P.; Liang, X.; Li, T. Small Target Detection Based on Noncoherent Radial Velocity Spectrum of High-Resolution Sea Clutter. *IEEE J. Sel. Top. Appl. Earth Obs. Remote Sens.* **2022**, *15*, 8719–8733. [CrossRef]

11. Xu, S.; Zhu, J.; Jiang, J.; Shui, P. Sea-Surface Floating Small Target Detection by Multifeature Detector Based on Isolation Forest. *IEEE J. Sel. Top. Appl. Earth Obs. Remote Sens.* **2021**, *14*, 704–715. [CrossRef]
12. Zhang, Y.; Jiang, L.; Ewe, H.T. A Novel Data-Driven Modeling Method for the Spatial–Temporal Correlated Complex Sea Clutter. *IEEE Trans. Geosci. Remote Sens.* **2022**, *60*, 5104211. [CrossRef]
13. Xue, J.; Liu, J.; Xu, S.; Pan, M. Adaptive Detection of Radar Targets in Heavy-Tailed Sea Clutter with Lognormal Texture. *IEEE Trans. Geosci. Remote Sens.* **2022**, *60*, 5108411. [CrossRef]
14. Madjidi, H.; Laroussi, T.; Farah, F. A Robust and Fast CFAR Ship Detector Based on Median Absolute Deviation Thresholding for SAR Imagery in Heterogeneous Log-Normal Sea Clutter. *Signal Image Video Process.* **2023**, *17*, 2925–2931. [CrossRef]
15. Weinberg, G.V.; Bateman, L.; Hayden, P. Development of Non-Coherent CFAR Detection Processes in Weibull Background. *Digit. Signal Process.* **2018**, *75*, 96–106. [CrossRef]
16. He, X.; Xu, Y.; Liu, M.; Hao, C.; Hou, C. Adaptive Estimation of K-Distribution Shape Parameter Based on Fuzzy Statistical Normalization Processing. *IEEE Trans. Aerosp. Electron. Syst.* **2022**, *58*, 4566–4577. [CrossRef]
17. Huang, P.; Zou, Z.; Xia, X.G.; Liu, X.; Liao, G. A Statistical Model Based on Modified Generalized-K Distribution for Sea Clutter. *IEEE Geosci. Remote Sens. Lett.* **2022**, *19*, 8015805. [CrossRef]
18. Fan, Y.; Chen, D.; Tao, M.; Su, J.; Wang, L. Parameter Estimation for Sea Clutter Pareto Distribution Model Based on Variable Interval. *Remote Sens.* **2022**, *14*, 2326. [CrossRef]
19. Xu, X.; Zhang, Y.; Li, X.; Yin, Z. KK Distribution Modeling with L Band Low Grazing Sea Clutter. *Syst. Eng. Electron.* **2014**, *36*, 1304–1308.
20. Rosenberg, L.; Watts, S.; Bocquet, S. Application of the K+Rayleigh Distribution to High Grazing Angle Sea-Clutter. In Proceedings of the 2014 International Radar Conference, Lille, France, 13–17 October 2014; pp. 1–6.
21. Wang, R.; Li, X.; Ma, H.; Zhang, H. Detection of Small Target in Sea Clutter via Multiscale Directional Lyapunov Exponents. *Sens. Rev.* **2019**, *39*, 752–762. [CrossRef]
22. Bocquet, S.; Rosenberg, L.; Gierull, C.H. Parameter Estimation for a Compound Radar Clutter Model with Trimodal Discrete Texture. *IEEE Trans. Geosci. Remote Sens.* **2020**, *58*, 7062–7073. [CrossRef]
23. Yang, L.; Liu, Y.; Yang, W.; Su, X.; Shen, Q. A Clutter Parameter Estimation Method Based on Origin Moment Derivation. *Remote Sens.* **2023**, *15*, 1551. [CrossRef]
24. Zhang, Y.; Yin, Y.; Li, H.; Wu, Z. Research on Amplitude Statistics of L-Band Low Grazing Angle Sea Clutter. *J. Electron. Inf. Technol.* **2014**, *36*, 1044–1048.
25. Liu, H.; Song, J.; Xiong, W.; Cui, Y.; Lv, Y.; Liu, J. Analysis of Amplitude Statistical and Correlation Characteristics of High Grazing Angle Sea-Clutter. *J. Eng.* **2019**, *2019*, 6829–6833. [CrossRef]
26. Mezache, A.; Chalabi, I. Estimation of the RiIG-Distribution Parameters Using the Artificial Neural Networks. In Proceedings of the 2013 IEEE International Conference on Signal and Image Processing Applications, Melaka, Malaysia, 8–10 October 2013; pp. 291–296.
27. Machado Fernández, J.R.; Bacallao Vidal, J.D.L.C.; Chávez Ferry, N. A Neural Network Approach to Weibull Distributed Sea Clutter Parameter's Estimation. *Intel. Artif.* **2015**, *18*, 3–13. [CrossRef]
28. Wang, G.; Wang, C.; Liu, C.; Liu, N.; Ding, H. Amplitude Distribution Parameter Estimation Method of Sea Clutter Using Neural Network. *J. Nav. Aviat. Univ.* **2019**, *34*, 480–487.
29. Xue, J.; Sun, M.; Liu, J.; Xu, S.; Pan, M. Shape Parameter Estimation of K-Distributed Sea Clutter Using Neural Network and Multisample Percentile in Radar Industry. *IEEE Trans. Ind. Inform.* **2023**, *19*, 7602–7612. [CrossRef]
30. Song, C.; Xiuwen, L. Statistical Analysis of X-Band Sea Clutter at Low Grazing Angles. In Proceedings of the 2020 International Conference on Big Data & Artificial Intelligence & Software Engineering (ICBASE), Bangkok, Thailand, 30 November–1 October 2020; pp. 141–144.
31. Zhao, X.; Han, J.; Zhang, X.; Zhang, J.; Li, P. Sea Clutter Measurement Test and Amplitude Characteristics Analysis in the South China Sea Nearshore Area. *J. Phys. Conf. Ser.* **2023**, *2486*, 012022. [CrossRef]
32. Ma, L. Research on Sea Clutter Characteristics Based on Deep Learning and Marine Environmental Parameters. Ph.D. Dissertation, Xidian University, Xi'an, China, 2021.
33. Hua, Z.; Zhang, J.; Yin, B.; Wang, Y.; Zhang, Y. An Integrated Prediction Method for Sea Clutter Amplitude Distribution in Complex Spatio-Temporal Scenarios. *Chin. J. Radio Sci.* **2023**, *39*, 1–8. [CrossRef]
34. Liu, N.; Dong, Y.; Wang, G.; Ding, H.; Huang, Y.; Guan, J.; Chen, X.; He, Y. Sea-Detecting X-Band Radar and Data Acquisition Program. *J. Radars* **2019**, *8*, 656–667.
35. Liu, N.; Ding, H.; Huang, Y.; Dong, Y.; Wang, G.; Dong, K. Annual Progress of the Sea-detecting X-band Radar and Data Acquisition Program. *J. Radars* **2021**, *10*, 173–182. [CrossRef]
36. Guan, J.; Liu, N.; Wang, G.; Ding, H.; Dong, Y.; Huang, Y.; Tian, K.; Zhang, M. Sea-detecting Radar Experiment and Target Feature Data Acquisition for Dual Polarization Multistate Scattering Dataset of Marine Targets. *J. Radars* **2023**, *12*, 456–469. [CrossRef]
37. Zhang, Y.; Yang, Q. An Overview of Multi-Task Learning. *Natl. Sci. Rev.* **2018**, *5*, 30–43. [CrossRef]
38. Vandenhende, S.; Georgoulis, S.; Gansbeke, W.V.; Proesmans, M.; Dai, D.; Gool, L.V. Multi-Task Learning for Dense Prediction Tasks: A Survey. *IEEE Trans. Pattern Anal. Mach. Intell.* **2022**, *44*, 3614–3633. [CrossRef] [PubMed]
39. Kieu, N.; Nguyen, K.; Nazib, A.; Fernando, T.; Fookes, C.; Sridharan, S. Multimodal Colearning Meets Remote Sensing: Taxonomy, State of the Art, and Future Works. *IEEE J. Sel. Top. Appl. Earth Obs. Remote Sens.* **2024**, *17*, 7386–7409. [CrossRef]

40. Zhang, Y.; Yang, Q. A Survey on Multi-Task Learning. *IEEE Trans. Knowl. Data Eng.* **2022**, *34*, 5586–5609. [CrossRef]
41. Wang, H.; Jin, X.; Du, Y.; Zhang, N.; Hao, H. Adaptive Hard Parameter Sharing Method Based on Multi-Task Deep Learning. *Mathematics* **2023**, *11*, 4639. [CrossRef]
42. Pahari, N.; Shimada, K. Multi-Task Learning Using BERT with Soft Parameter Sharing Between Layers. In Proceedings of the 2022 Joint 12th International Conference on Soft Computing and Intelligent Systems and 23rd International Symposium on Advanced Intelligent Systems (SCIS&ISIS), Ise, Japan, 29 November–2 December 2022; pp. 1–6.
43. Lin, B.; Ye, F.; Zhang, Y.; Tsang, I.W. Reasonable Effectiveness of Random Weighting: A Litmus Test for Multi-Task Learning. *arXiv* **2021**, arXiv:2111.10603. [CrossRef]
44. Li, B.; Dong, A. Multi-Task Learning with Attention: Constructing Auxiliary Tasks for Learning to Learn. In Proceedings of the 2021 IEEE 33rd International Conference on Tools with Artificial Intelligence (ICTAI), Washington, DC, USA, 1–3 November 2021; pp. 145–152.
45. Choudhary, P.; Pathak, P. A Review of Convolution Neural Network Used in Various Applications. In Proceedings of the 2021 5th International Conference on Information Systems and Computer Networks (ISCON), Mathura, India, 22–23 October 2021; pp. 1–5.
46. Li, Y.; Ye, C.; Ge, Y.; Junior, J.M.; Gonçalvese, W.N.; Li, J. Identifying Building Rooftops in Hyperspectral Imagery Using CNN With Pure Pixel Index. *IEEE J. Sel. Top. Appl. Earth Obs. Remote Sens.* **2021**, *14*, 12022–12034. [CrossRef]
47. Kiranyaz, S.; Avci, O.; Abdeljaber, O.; Ince, T.; Gabbouj, M.; Inman, D.J. 1D Convolutional Neural Networks and Applications: A Survey. *Mech. Syst. Signal Process.* **2021**, *151*, 107398. [CrossRef]
48. Chaubey, V.; Nair, M.S.; Pillai, G.N. Gene Expression Prediction Using a Deep 1D Convolution Neural Network. In Proceedings of the 2019 IEEE Symposium Series on Computational Intelligence (SSCI), Xiamen, China, 6–9 December 2019; pp. 1383–1389.
49. Song, P.; Geng, C.; Li, Z. Research on Text Classification Based on Convolutional Neural Network. In Proceedings of the 2019 International Conference on Computer Network, Electronic and Automation (ICCNEA), Xi'an, China, 27–29 September 2019; pp. 229–232.
50. Martynov, G. Weighted Cramer-von Mises Test with Estimated Parameters. *Commun. Stat. Theory Methods* **2011**, *40*, 3569–3586. [CrossRef]
51. Chan, H.C. Radar Sea-Clutter at Low Grazing Angles. In *IEE Proceedings F Radar and Signal Processing*; IET: Stevenage, UK, 1990; Volume 137, p. 102.
52. Iskander, D.R.; Zoubir, A.M. Estimation of the Parameters of the K-Distribution Using Higher Order and Fractional Moments. *IEEE Trans. Aerosp. Electron. Syst.* **1999**, *35*, 1453–1457. [CrossRef]